

Multi-user Beamforming in RIS-aided Communications and Experimental Validations

Zhibo Zhou, Haifan Yin, *Member, IEEE*, Li Tan, Ruikun Zhang, Kai Wang, Yingzhuang Liu

Abstract—Reconfigurable intelligent surface (RIS) is a promising technology for future wireless communications due to its capability of optimizing the propagation environments. Nevertheless, in literature, there are few prototypes serving multiple users. In this paper, we propose a whole flow of channel estimation and beamforming design for RIS, and set up an RIS-aided multi-user system for experimental validations. Specifically, we combine a channel sparsification step with generalized approximate message passing (GAMP) algorithm, and propose to generate the measurement matrix as Rademacher distribution to obtain the channel state information (CSI). To generate the reflection coefficients with the aim of maximizing the spectral efficiency, we propose a quadratic transform-based low-rank multi-user beamforming (QTLM) algorithm. Our proposed algorithms exploit the sparsity and low-rank properties of the channel, which has the advantages of light calculation and fast convergence. Based on the universal software radio peripheral devices, we built a complete testbed working at 5.8 GHz and implemented all the proposed algorithms to verify the possibility of RIS assisting multi-user systems. Experimental results show that the system has obtained an average spectral efficiency increase of 13.48 bps/Hz, with respective received power gains of 26.6 dB and 17.5 dB for two users, compared with the case when RIS is powered-off.

Index Terms—Reconfigurable intelligent surface (RIS), multi-user beamforming, channel estimation, experimental validations.

I. INTRODUCTION

RECONFIGURABLE intelligent surface (RIS) is anticipated to be a potential key technology for future 6G mobile communication systems due to its great capability of manipulating the electromagnetic environment [1]–[3]. By individually configuring the reflection coefficient of each element, RIS can efficiently execute a multitude of essential functions in communication, e.g., reflecting the incident radio signal towards a desired direction to facilitate additional beamforming, enhancing the rank of the channel to attain the full multiplexing gain [4], suppressing co-channel interference [5], etc, while maintaining a low energy consumption and cost-effective hardware deployment. Furthermore, as the central frequency of wireless communication systems advances towards the mmWave/subTHz range, the RIS emerges as a potential attempt to play an increasingly pivotal role in the future. This

potential stems from the pronounced power attenuation in free space exhibited by high-frequency electromagnetic waves, as well as the high penetration loss. The attractive benefits offered by RIS have spurred researches in various perspectives, such as element designs [6]–[10], path loss modelings [11]–[13], and transmission protocols [14]–[16].

In practical terms, the challenge of RIS deployments lies mainly in how to configure it correctly to maximize its performance gains [17]–[19]. Nevertheless, as far as our current understanding goes, only a limited number of prototypes have incorporated adaptive beamforming algorithms, and even fewer have ventured into the realm of more complex multi-user scenarios. The reasons for this phenomenon include overly desirable preconditions, high complexity, etc. In existing prototypes of RIS-aided wireless systems, there are four main methods to configure the reflection coefficients: 1) Beam-searching-based method, 2) Iterative algorithm, 3) Codeword design from location information, 4) Beamforming based on the estimated channel state information (CSI).

For a beam-searching-based scheme, the work in [20] chooses to observe the conditional expectation of the received power to select the best configuration within a randomly generated reflection coefficient set, which can be extended to multi-user scenarios by substituting the performance indicator with the sum-rate of the whole system. In the second category, the authors in [10] leverage extra feedback links to acquire a performance indicator, e.g., Reference Signal Received Power (RSRP). Through activating different groups of elements and observing the variations of the RSRP, the iterative algorithm facilitates a step-by-step enhancement in the received power for an individual user within real-world scenarios. This approach maintains a relatively high level of performance while exhibiting a low complexity. In the third category, the main theory of designing codeword is to guarantee that the signal reflected by each element adds up coherently at the receiver, which can be implemented with the help of steering vector to compensate the phase shifting of the multiple paths between the transmitter and the receiver. The authors in [21] attached cameras to the system to assist in obtaining location information and calculated the phase to be compensated for each element. The authors in [22] proposed a method of Riemann manifold optimization to generate codewords for the far-field scenarios. In the last category, an adaptive beamforming algorithm based on CSI estimated from Matching Pursuit (MP) algorithm was proposed and applied into a single-user scenario to verify the capability of RIS in [23].

Most early designs in RIS prototype avoided complex algorithms to verify the steering capability of RIS technology

Z. Zhou, H. Yin, L. Tan, R. Zhang, K. Wang, Y. Liu are with the School of Electronic Information and Communications, Huazhong University of Science and Technology, Wuhan, China. E-mail: {z Zhou, yin, ltan, zhangrk, kaiw, liuyz}@hust.edu.cn.

The corresponding author is Li Tan.

This work was supported in part by the National Key Research and Development Program of China under Grant 2020YFB1806904, in part by by the National Natural Science Foundation of China under Grants 62071191, 62071192 and 1214110.

in a single-user case. Nevertheless, in order to characterize the capability of RIS serving multi-user wireless communication systems, the configuration of RIS requires a more strict method. Considering the need of applying in the real prototype, we divide the problem of configuring RIS into two separate sub-problems, i.e., channel estimation and multi-user beamforming.

The channel estimation problem in an RIS-aided system is tough due to the passive nature of the elements and the high dimensionality of the entire surface. Early algorithm research works focused on simple signal processing techniques such as the Least Square/Linear Minimum Mean Square Error (LS/LMMSE) estimation method based on pilots. These traditional methods do not effectively solve the challenge of high dimensionality. To further reduce the dimensionality, one possible method is to exploit the structure properties of the channel vector [24]. Along this line, we introduce the angular domain channel model and formulate the channel estimation with Compressed Sensing (CS) terminology. Specifically, we propose to generate the measurement matrix as Rademacher distribution to match the 1-bit quantized RIS prototype. Moreover, we utilize Expectation Maximization-Generalized Approximate Message Passage (EM-GAMP) algorithm to obtain the cascaded CSI in RIS model. Based on the estimated CSI, the central mission of multi-user beamforming algorithms is to design the reflection coefficients of each RIS element by formulating multi-user beamforming as an optimization in a mathematical expression, to reach different goals according to different application scenarios. However, the main challenges of these algorithms when applied to practical prototypes includes the non-convexity introduced by the objective function and quantized constraints, and the high dimensionality. To address these two problems, we introduce the iterative framework and exploit the low-rank property [25] in the channel model respectively. The proposed quadratic transform-based low-rank multi-user beamforming (QTLM) algorithm allows us to update the auxiliary variables of each sub-problem until the spectral efficiency of the whole system converges. Due to the non-decreasing property and a determined upper bound of the objective function, the algorithm is assured to converge at a local optimal point. The proposed method has the possibility of applying to prototypes and the advantages of light calculation and fast convergence.

The main contributions of this paper are summarized as follows:

- To the best of our knowledge, few works have been done on RIS-aided multi-user prototypes. We have designed and implemented an RIS-aided multi-user wireless communication system based on Universal Software Radio Peripheral (USRP) devices. Through a series of experiments, the results unequivocally reveal a significant augmentation in the spectral efficiency of the entire system after the configuration of the RIS. Furthermore, we conducted measurements on the radiation pattern of the codeword generated from our algorithms, and the findings indicate the potential application of the algorithm in a multi-user scenario and its ability to generate multiple beams.

- We have designed the whole workflow of the channel estimation and multi-user beamforming algorithms which can be employed in our RIS prototypes. Specifically, we introduce the angular domain channel model and formulate the channel estimation problem into CS terminology. In order to match our 1-bit quantized RIS prototype, we propose to generate the sensing matrix as Rademacher distribution and combine it with the generalized approximate message passing (GAMP) algorithm. Based on the estimated channel vector, we formulate the multi-user beamforming optimization problem and propose a quadratic transform-based low-rank multi-user beamforming (QTLM) algorithm to compute the reflection coefficients. In the process of the algorithms, we exploit the low-rank property in the model to reduce the complexity and accelerate the convergence.
- Since the algorithm we have developed requires an accurate noise power value throughout its iteration, the noise floor in radio frequency (RF) devices is not sufficient for characterizing it. To address this issue, we introduce a novel approach that involves compensating the noise power through the utilization of the Receive Modulation Error Ratio (RxMER). This correction factor considers the impairments present in RF chains, thereby enhancing the precision of the noise power estimation. By implementing this correction, the received power gain of a two-user system attains an average improvement of 10 dB, underscoring the efficacy of this corrective technique.

The remainder of this paper is organized as follows: Section II introduces the system model. The channel estimation problem is formulated and the related algorithm to solve it is described in Section III. In Section IV, we formulate the passive beamforming optimization problem in multi-user system, and develop an iterative algorithm that could be applied to the prototype. The main results obtained in our testbed are presented in Section V. Section VI concludes this paper.

Notations: We use the boldface lower-case letter to denote a vector, the boldface upper-case letter a matrix. Let $(\mathbf{X})^T$, $(\mathbf{X})^*$, and $(\mathbf{X})^H$ denote the transpose, conjugate, and conjugate transpose of a matrix \mathbf{X} respectively. $\|\mathbf{x}\|_0$ and $\|\mathbf{x}\|_2$ denote the ℓ_0 -norm and the ℓ_2 -norm of a vector \mathbf{x} respectively. Denote the phase vector of a complex vector \mathbf{x} by $\angle \mathbf{x}$. And $\text{diag}(\boldsymbol{\alpha})$ denotes a diagonal matrix with vector $\boldsymbol{\alpha}$ at the main diagonal. The Kronecker product of two matrices \mathbf{X} and \mathbf{Y} is denoted by $\mathbf{X} \otimes \mathbf{Y}$. For a complex number x , $\Re(x)$ denotes its real part, and $|x|$ denotes its absolute value. For a random variable $X \sim \mathcal{CN}(\mu, \sigma^2)$ represents that X follows Circularly Symmetric Complex Gaussian distribution (CSCG) with expectation μ and variance σ^2 .

II. SYSTEM MODEL

Consider an RIS-aided multi-user wireless communication system as shown in Fig. 1, which consists of a single-antenna BS and K users, equipped with a single antenna as well. The RIS is composed of $N = N_y N_z$ elements arranged in a uniform planer array (UPA), where N_y and N_z are the

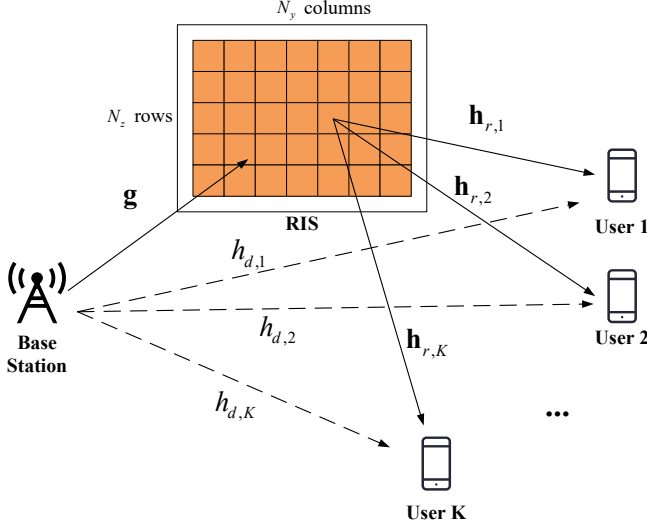


Fig. 1. An illustration of an RIS-aided multi-user wireless communication system.

numbers of elements in the y -axis and the z -axis respectively. The channels from the BS to the k -th user (also known as direct link), from the BS to the RIS, and from the RIS to the k -th user are denoted by $h_{d,k} \in \mathbb{C}$, $\mathbf{g} \in \mathbb{C}^{N \times 1}$ and $\mathbf{h}_{r,k} \in \mathbb{C}^{1 \times N}$ respectively, with $k = 1, \dots, K$. The reflection coefficients of the RIS elements are denoted by $\boldsymbol{\theta} = [\theta_1 \ \theta_2 \ \dots \ \theta_N]^T$. In engineering practice, the phase shifting of the element of the RIS is quantized to discrete bits. The phase shifting of a τ -bit quantized RIS takes 2^τ values, i.e., $\theta_n = e^{j\varphi_n}$, where $\varphi_n \in \{0, \frac{1}{2^\tau}2\pi, \dots, \frac{2^\tau-1}{2^\tau}2\pi\}$, $n = 1, \dots, N$.

In our model, the direct channel is assumed Gaussian and denoted by $h_{d,k} \sim \mathcal{CN}(0, \sigma_k^2)$, where σ_k^2 is the power of the channel of the k -th user. The widely used Saleh-Valenzuela channel model [26], [27] is adopted to represent the channel \mathbf{g} between the BS and the RIS as

$$\mathbf{g} = \sum_l^{L_g} \beta_l^g \boldsymbol{\alpha}(\vartheta_l^g, \varphi_l^g), \quad (1)$$

where L_g denotes the number of paths between the BS and the RIS, β_l^g is the complex path gain of the l -th path, $\vartheta_l^g(\varphi_l^g)$ denote the azimuth (elevation) angle of the l -th path at the RIS.

Similarly, the channel between the RIS and the k -th user is modeled as

$$\mathbf{h}_{r,k} = \sum_l^{L_k} \beta_l^k \boldsymbol{\alpha}^T(\vartheta_l^k, \varphi_l^k), \quad (2)$$

where L_k is the number of paths between the RIS and the k -th user, β_l^k is the complex path gain of the l -th path, $\vartheta_l^k(\varphi_l^k)$ denotes the azimuth (elevation) angle at the RIS. Furthermore, $\boldsymbol{\alpha}(\vartheta, \varphi)$ denotes far-field steering vector for RIS and can be written as [28]

$$\boldsymbol{\alpha}(\vartheta, \varphi) = \boldsymbol{\alpha}_y(\vartheta, \varphi) \otimes \boldsymbol{\alpha}_z(\varphi), \quad (3)$$

where $\boldsymbol{\alpha}_y$ and $\boldsymbol{\alpha}_z$ denotes the array response vector of a

uniform linear array along the y -axis and z -axis respectively:

$$\boldsymbol{\alpha}_y(\vartheta, \varphi) = \left[1, e^{-j2\pi \frac{d_y}{\lambda} \sin(\vartheta) \sin(\varphi)}, \dots, e^{-j2\pi \frac{d_y}{\lambda} \sin(\vartheta) \sin(\varphi)(N_y-1)} \right]^T, \quad (4)$$

$$\boldsymbol{\alpha}_z(\varphi) = \left[1, e^{-j2\pi \frac{d_z}{\lambda} \cos(\varphi)}, \dots, e^{-j2\pi \frac{d_z}{\lambda} \cos(\varphi)(N_z-1)} \right]^T, \quad (5)$$

where d_y and d_z are y -axis and z -axis element spacing respectively, which typically satisfy $d_y(d_z) \leq \lambda/2$ in RIS model, and λ is the wave-length. The distance boundary of near field and far field is defined as [11]

$$B = \frac{2N_y N_z d_y d_z}{\lambda}. \quad (6)$$

Denote the downlink transmitted signal to the k -th user by s_k , and normalize the power to $|s_k| = 1$. The received signal of the k -th user is expressed as

$$y_k = \underbrace{(h_{d,k} s_k)}_{\text{direct link}} + \underbrace{\mathbf{h}_{r,k} \text{diag}(\boldsymbol{\theta}) \mathbf{g} s_k}_{\text{RIS-aided link}} + n_k, \quad (7)$$

where $n_k \sim \mathcal{CN}(0, \sigma^2)$. Let $\mathbf{h}_k = \text{diag}(\mathbf{h}_{r,k}) \mathbf{g} \in \mathbb{C}^{N \times 1}$, then the received signal is

$$y_k = (h_{d,k} + \boldsymbol{\theta}^T \text{diag}(\mathbf{h}_{r,k}) \mathbf{g}) s_k + n_k \quad (8)$$

$$= (h_{d,k} + \boldsymbol{\theta}^T \mathbf{h}_k) s_k + n_k. \quad (9)$$

In this equation, the RIS-aided link in (9) can be divided into two parts, the first one is a vector of reflection coefficients, and the second only contains the fading channel, which is known as cascaded channel as well. Most studies assume that the direct link $h_{d,k}$ is blocked by obstacles and ignores its effect on the received signal. However, our experimental results show that in the real environments this link could be small in power, compared with the RIS-aided link, yet has an impact on how to configure the reflection coefficients of RIS. As a result, this part of the information is needed in our experiment.

III. CS-BASED CHANNEL ESTIMATION METHOD

Most passive beamforming design research assumes perfect CSI and designs the beamforming algorithm based on this. In practice, however, the estimation of the cascaded channel is one of the major challenges of RIS. In our experiments, both the direct link channel and the cascaded channel need to be estimated.

The direct link channel estimate problem can be solved by utilizing conventional LS methods once we assume that RIS absorbs incident electromagnetic waves. The main difficulty lies in the estimation of the cascaded channel due to the high dimension of the RIS board and the passive properties of the RIS element. To reduce the impact of pilot overhead on system throughput, we introduce an angular domain channel model. For the channel model in (9), the virtual angular expression is $\mathbf{h}_k^a = \mathbf{D}_N \mathbf{h}_k$, where $\mathbf{D}_N = \mathbf{D}_{N_y} \otimes \mathbf{D}_{N_z}$ is a Kronecker product of two discrete Fourier transform (DFT) matrices with dimensions N_y and N_z . By taking this transform, only a few coefficients in \mathbf{h}_k^a have relatively high magnitude, and other coefficients are close to zero, i.e., the angular-domain vector \mathbf{h}_k^a is sparse, thus converting the original problem

into estimating a sparse vector and significantly reducing the dimension of the signal to be estimated. The detailed algorithm is summarized below.

Assume that we estimate channel vector in P time slots, with $P \ll N$. Denote the symbols transmitted in P time slots to the k -th user by $\mathbf{s} = [s_1 \ s_2 \ \cdots \ s_P]^T$, the reflection coefficients of RIS in the p -th slot are represented by θ_p , $p = 1, \dots, P$. All reflection coefficients vectors in P slots form a matrix $\Theta = [\theta_1 \ \theta_2 \ \cdots \ \theta_P] \in \mathbb{C}^{N \times P}$. For the k -th user, the received signals in P slots after removing the impact of the direct link are represented as

$$\mathbf{y}_k = \begin{bmatrix} \theta_1^T \mathbf{h}_k s_1 + n_{k,1} \\ \theta_2^T \mathbf{h}_k s_2 + n_{k,2} \\ \vdots \\ \theta_P^T \mathbf{h}_k s_P + n_{k,P} \end{bmatrix} = \begin{bmatrix} \theta_1^T \mathbf{h}_k s_1 \\ \theta_2^T \mathbf{h}_k s_2 \\ \vdots \\ \theta_P^T \mathbf{h}_k s_P \end{bmatrix} + \mathbf{n}_k, \quad (10)$$

where \mathbf{n}_k is a vector of additive white Gaussian noise. Denote $\mathbf{M} = \Theta^T \mathbf{D}_N^H$ and we have

$$\mathbf{y}_k = \mathbf{M} \mathbf{h}_k^a + \mathbf{n}_k. \quad (11)$$

The channel estimation problem is to reconstruct the channel vector \mathbf{h}_k^a from the known matrix \mathbf{M} and the received signal vector \mathbf{y}_k . With the sparse structure of \mathbf{h}_k^a , we can utilize CS framework to solve it. Formulate as an optimization problem:

$$\begin{aligned} \min_{\mathbf{h}_k^a} \quad & \|\mathbf{h}_k^a\|_0 \\ \text{s.t.} \quad & \|\mathbf{y}_k - \mathbf{M} \mathbf{h}_k^a\|_2^2 \leq \epsilon, \end{aligned} \quad (12)$$

where ϵ is the tolerance upper bound related to noise power. In CS terminology, \mathbf{M} is the $P \times N$ sensing matrix, \mathbf{y}_k is the $P \times 1$ measurement vector. The sensing matrix should satisfy Restricted Isometry Property (RIP) to recover sparse signal [29], which guarantees that the columns of \mathbf{M} are nearly orthonormal. In particular, it is shown that some random matrices such as Gaussian matrix, Bernoulli matrix, etc, satisfy the RIP with exponentially high probability [30]. In our experimental model, since the RIS is quantified to one bit, the possible values of reflection coefficient ($\theta_{i,j} \in \{1, -1\}$) match a Rademacher distribution. Hence we propose to randomly generate Θ as a Rademacher matrix. Let $\theta_{i,j}$ be the i, j -th element in Θ , the probability mass function of $\theta_{i,j}$ is

$$f(\theta_{i,j}) = \begin{cases} \frac{1}{2} & \text{if } \theta_{i,j} = 1, \\ \frac{1}{2} & \text{if } \theta_{i,j} = -1, \\ 0 & \text{otherwise.} \end{cases} \quad (13)$$

Compared with the randomized distribution with continuous values, the Rademacher matrix retains less information after projecting into low-dimensional space since the available values of this distribution is limited in $\{1, -1\}$, resulting in performance loss in signal recovery algorithms. As a result, this loss stems unavoidably from the quantization limitation of RIS hardware system.

Mathematically, there are many methods to solve CS problems, such as Orthogonal Matching Pursuit (OMP), Basis Pursuit (BP), etc. Different algorithms will converge to different results (maybe local optimal) and have different complexity.

The performance of the recovery algorithm is measured with Normalized Mean Squared Error (NMSE) defined below:

$$\zeta = \frac{1}{K} \sum_{k=1}^K \frac{\|\mathbf{h}_k^a - \tilde{\mathbf{h}}_k^a\|_2^2}{\|\mathbf{h}_k^a\|_2^2}, \quad (14)$$

where \mathbf{h}_k^a is the actual value and $\tilde{\mathbf{h}}_k^a$ is the estimated value of the channel vector of the k -th user. In practice, we adopt the GAMP algorithm in the channel estimation, since it has the advantages of lightweight calculation and fast convergence. However, it also requires a prior information of the sparsity rate of the channel vector, which is unknown in real world. Therefore, we choose to combine it with the Expectation Maximization (EM) method to estimate the relevant parameters.

IV. MULTI-USER BEAMFORMING

A. Problem Formulation

Due to channel reciprocity in RIS-aided system in time division duplexing (TDD) mode [10], the uplink and downlink channels are equal. Based on the transmission model in (9), the received Signal-to-Noise Ratio (SNR) of the k -th user is computed by

$$\gamma_k = \frac{|h_{d,k} + \boldsymbol{\theta}^T \mathbf{h}_k|^2}{\sigma^2}. \quad (15)$$

Then the spectral efficiency of the whole broadcast communication system is defined as

$$f(\boldsymbol{\theta}) = \sum_{k=1}^K \log_2(1 + \gamma_k). \quad (16)$$

Our objective is to configure the reflection coefficients of RIS elements $\boldsymbol{\theta}$ to maximize the spectral efficiency under discrete constraints, namely passive beamforming design. Formulate an optimization problem:

$$\begin{aligned} \text{(P1)} \quad & \max_{\boldsymbol{\theta}} \quad f_1(\boldsymbol{\theta}) = \sum_{k=1}^K \log_2(1 + \gamma_k) \\ \text{s.t.} \quad & \theta_n \in \mathcal{F}_d \quad \forall n = 1, \dots, N. \end{aligned} \quad (17)$$

For such an optimization problem, both the objective function and the constraints are non-convex. We propose an iterative algorithm based on Lagrange dual transform and quadratic transform, reduce the original problem into convex one and derive the closed-form solution for each sub-problem, which highly reduces the complexity. The details of the algorithm are shown in the next subsection.

B. Proposed Quadratic Transform-based Low-rank Multi-user Beamforming Algorithm

To tackle logarithm in the objective function of (P1), we apply the Lagrangian dual transform [31], the problem (P1) can be equivalently written as

$$\begin{aligned} \text{(P1a)} \quad & \max_{\boldsymbol{\theta}, \boldsymbol{\alpha}} \quad f_{1a}(\boldsymbol{\theta}, \boldsymbol{\alpha}) \\ \text{s.t.} \quad & \theta_n \in \mathcal{F}_d \quad \forall n = 1, \dots, N, \end{aligned} \quad (18)$$

where $\boldsymbol{\alpha} = [\alpha_1 \ \alpha_2 \ \cdots \ \alpha_K]^T \in \mathbb{R}^K$ is the auxiliary variables for the received SNR γ_k , and a new objective function is defined:

$$f_{1a}(\boldsymbol{\theta}, \boldsymbol{\alpha}) = \sum_{k=1}^K \log_2(1 + \alpha_k) - \sum_{k=1}^K \alpha_k + \sum_{k=1}^K \frac{(1 + \alpha_k)\gamma_k}{1 + \gamma_k}. \quad (19)$$

In (P1a), when $\boldsymbol{\theta}$ is fixed, the optimization problem for $\boldsymbol{\alpha}$ is convex, thus by letting $\partial f_{1a}(\boldsymbol{\theta}, \boldsymbol{\alpha})/\partial \alpha_k = 0$, the optimal α_k is obtained:

$$\alpha_k^{\text{opt}} = \gamma_k. \quad (20)$$

Then for a fixed α_k , define $\tilde{\alpha}_k = 1 + \alpha_k$, the variables of the optimization problem, i.e., $\gamma_k, k = 1, \dots, K$, exist only in the third term in (19). The optimization problem is reduced to

$$(P2) \quad \begin{aligned} & \max_{\boldsymbol{\theta}} \quad f_2(\boldsymbol{\theta}) \\ & \text{s.t.} \quad \theta_n \in \mathcal{F}_d \quad \forall n = 1, \dots, N, \end{aligned} \quad (21)$$

where

$$f_2(\boldsymbol{\theta}) = \sum_{k=1}^K \frac{\tilde{\alpha}_k \gamma_k}{1 + \gamma_k}. \quad (22)$$

The problem (P2) is the sum of multiple-ratio fractional programming problem and non-convex for $\boldsymbol{\theta}$. Utilize the quadratic transform [31] and substitute (15) into (21), (P2) is equivalent to

$$(P2a) \quad \begin{aligned} \max_{\boldsymbol{\theta}, \boldsymbol{\varepsilon}} \quad f_{2a}(\boldsymbol{\theta}, \boldsymbol{\varepsilon}) &= \sum_{k=1}^K 2\sqrt{\tilde{\alpha}_k} \Re \{ \varepsilon_k^* (h_{d,k} + \boldsymbol{\theta}^T \mathbf{h}_k) \} \\ &\quad - \sum_{k=1}^K |\varepsilon_k|^2 (\sigma^2 + |h_{d,k} + \boldsymbol{\theta}^T \mathbf{h}_k|^2) \\ \text{s.t.} \quad \theta_n &\in \mathcal{F}_d, \end{aligned} \quad (23)$$

where $\boldsymbol{\varepsilon} = [\varepsilon_1 \ \cdots \ \varepsilon_K]^T \in \mathbb{C}^K$ is the auxiliary variable. Similarly, (P2a) for $\boldsymbol{\varepsilon}$ is convex, and by letting $\partial f_{2a}(\boldsymbol{\theta}, \boldsymbol{\varepsilon})/\partial \varepsilon_k = 0$, we derive the optimal value as

$$\varepsilon_k^{\text{opt}} = \frac{\sqrt{\tilde{\alpha}_k} (h_{d,k} + \boldsymbol{\theta}^T \mathbf{h}_k)}{\sigma^2 + |h_{d,k} + \boldsymbol{\theta}^T \mathbf{h}_k|^2}. \quad (24)$$

Then substitute (24) into $f_{2a}(\boldsymbol{\theta}, \boldsymbol{\varepsilon})$, we obtain

$$f_{2b}(\boldsymbol{\theta}) = -\boldsymbol{\theta}^T \mathbf{U} \boldsymbol{\theta}^* + 2\Re(\boldsymbol{\theta}^T \mathbf{v}) + C, \quad (25)$$

where

$$\mathbf{U} = \sum_{k=1}^K |\varepsilon_k|^2 \mathbf{h}_k \mathbf{h}_k^H, \quad (26)$$

$$\mathbf{v} = \sum_{k=1}^K \left(\sqrt{\tilde{\alpha}_k} \varepsilon_k^* \mathbf{h}_k - |\varepsilon_k|^2 h_{d,k} \mathbf{h}_k \right), \quad (27)$$

$$C = \sum_{k=1}^K \left(\sqrt{\tilde{\alpha}_k} \Re(\varepsilon_k^* h_{d,k}) - |\varepsilon_k|^2 \sigma^2 - |\varepsilon_k|^2 |h_{d,k}|^2 \right). \quad (28)$$

The optimization problem becomes

$$(P3) \quad \begin{aligned} & \max_{\boldsymbol{\theta}} \quad f_{2b}(\boldsymbol{\theta}) \\ & \text{s.t.} \quad \theta_n \in \mathcal{F}_d. \end{aligned} \quad (29)$$

Since for an arbitrary non-zero vector $\mathbf{x} \in \mathbb{C}^{N \times 1}$, $\mathbf{x}^H \mathbf{U} \mathbf{x} = \sum_{k=1}^K |\varepsilon_k|^2 |\mathbf{h}_k^H \mathbf{x}|^2 \geq 0$ always holds, $f_{2b}(\boldsymbol{\theta})$ is a quadratic concave function of $\boldsymbol{\theta}$. However, when considering the quantization in the RIS model, the constraints in (P3) are not convex, which is difficult to cope with. In our experiments, we may first compute an unquantized optimization result (i.e., adjust the constraints to $|\theta_n| = 1$) and then project it into the corresponding nearest bit. Moreover, the authors in [18] point out that even if we relax the constraints to $|\theta_n| \leq 1$, the optimization result will be close to $|\theta_n| = 1$ in the end, indicating that the two constraint schemes ($|\theta_n| \leq 1$ and $|\theta_n| = 1$) are almost equivalent in this condition. In this perspective, to solve (P3), we develop the following steps:

- First, solve a convex quadratically constrained quadratic program (QCQP) problem (P4) as follows

$$(P4) \quad \begin{aligned} & \max_{\boldsymbol{\theta}} \quad f_{2b}(\boldsymbol{\theta}) \\ & \text{s.t.} \quad \theta_n \in \mathcal{F}_c \quad \forall n = 1, \dots, N, \end{aligned} \quad (30)$$

where $\mathcal{F}_c = \{\theta_n | |\theta_n| \leq 1, n = 1, \dots, N\}$. Define $\mathbf{e}_i = [0, \dots, 0, 1, 0, \dots, 0]$, and $\mathbf{T}_i = \text{diag}(\mathbf{e}_i)$ is positive definite, thus \mathcal{F}_c is equivalent to N independent constraints:

$$\boldsymbol{\theta}^H \mathbf{T}_i \boldsymbol{\theta} \leq 1, \quad \forall i = 1, \dots, N. \quad (31)$$

It is clear that the feasible set \mathcal{F}_c is convex, thus the problem (P4) is convex. The solvers in convex optimization (e.g., CVX toolbox) can obtain the optimal solutions $\boldsymbol{\theta}^{\mathcal{F}_c}$ which obeys the rule that the modulus is close to one. There may be problems of high computational complexity without considering any preconditions of the original problems in the solving process of solvers. To address this issue, we propose a workflow below utilizing the low-rank properties to reduce complexity.

- Second, project all reflection coefficients to discrete bits according to the rules of closest point projection, i.e.,

$$\theta_n^{\mathcal{F}_d} = \arg \min_{\phi_n \in \mathcal{F}_d} |\phi_n - \theta_n^{\mathcal{F}_c}|. \quad (32)$$

The matrix $\mathbf{U} \in \mathbb{C}^{N \times N}$ is the sum of K rank-1 matrices, and thus satisfies $\text{rank}(\mathbf{U}) \leq K \ll N$. Perform Eigenvalue Decomposition (EVD) on \mathbf{U} , i.e.,

$$\mathbf{U} = \mathbf{P}^H \mathbf{D} \mathbf{P}, \quad (33)$$

where \mathbf{D} is a diagonal matrix. Denote the entries on its diagonal by $\mathbf{d} = [d_1 \ d_2 \ \cdots \ d_K \ 0 \ \cdots]$. The objective function is transformed into

$$f_{2b}(\boldsymbol{\theta}) = -\boldsymbol{\theta}^T \mathbf{P}^H \mathbf{D} \mathbf{P} \boldsymbol{\theta}^* + 2\Re(\boldsymbol{\theta}^T \mathbf{v}) + C. \quad (34)$$

Denote the new optimization variables as

$$\boldsymbol{\omega} = \mathbf{P} \boldsymbol{\theta}^*. \quad (35)$$

Since the unitary matrix does not affect the constraints, the optimization problem is further transformed into

$$\begin{aligned} & \max \quad f_{2c}(\boldsymbol{\omega}) = -\boldsymbol{\omega}^H \mathbf{D} \boldsymbol{\omega} + 2\Re(\boldsymbol{\omega}^H \mathbf{P} \mathbf{v}) + C \\ & \text{s.t.} \quad \omega_n \in \mathcal{F}_c. \end{aligned} \quad (36)$$

Since the matrix \mathbf{D} is diagonal, the term $\boldsymbol{\omega}^H \mathbf{D} \boldsymbol{\omega}$ in (36) can

be rewritten as

$$\boldsymbol{\omega}^H \mathbf{D} \boldsymbol{\omega} = \sum_{i=1}^N \omega_i^* d_i \omega_i = \sum_{i=1}^K \omega_i^* d_i \omega_i. \quad (37)$$

Denote $\mathbf{P} \mathbf{v}$ by \mathbf{b} and the term $2\Re(\boldsymbol{\omega}^H \mathbf{P} \mathbf{v})$ is represented by

$$2\Re(\boldsymbol{\omega}^H \mathbf{P} \mathbf{v}) = 2\Re\left(\sum_{i=1}^N \omega_i^* b_i\right). \quad (38)$$

Thus the closed-form solution to (36) is

$$\omega_k = \begin{cases} \frac{b_k}{d_k} & k = 1, \dots, K, \\ e^{i\angle b_k} & k = K + 1, \dots, N. \end{cases} \quad (39)$$

The computed reflection coefficients are obtained according to (35). The final step is the closest point projection, which concludes the flow of a single iteration. Denote the result in the i -th iteration by $\boldsymbol{\theta}^i$, the updating flag is whether the objective function of (P3) is increasing, which also guarantees the non-decreasing property of the objective function of (P1). The procedures of this algorithm are summarized below.

Algorithm 1 Proposed Quadratic Transform-based Low-rank Multi-user Beamforming Algorithm (QTLM)

Input: Randomly generated initial reflection coefficients vector $\boldsymbol{\theta}^0 \in \mathcal{F}_3$, the maximum number of iterations t_{\max} , the direct link channel coefficient by LS method and the cascaded channel vector estimated by solving (12).

Output: Computed reflection coefficients $\boldsymbol{\theta}^*$.

- 1: $\boldsymbol{\theta}^* \leftarrow \boldsymbol{\theta}^0$
- 2: **for all** $t = 1, \dots, t_{\max}$ **do**
- 3: Update $\boldsymbol{\alpha}^i$ according to (20) and (15);
- 4: Update $\boldsymbol{\varepsilon}^i$ according to (24) and calculated $\boldsymbol{\alpha}^i$;
- 5: Calculate a continuous result by solving (P4);
- 6: Project the continuous results into quantized one according to (32), denoted by $\boldsymbol{\theta}^i$;
- 7: **if** $f_{2b}(\boldsymbol{\theta}^i) > f_{2b}(\boldsymbol{\theta}^*)$ **then**
- 8: $\boldsymbol{\theta}^* \leftarrow \boldsymbol{\theta}^i$;
- 9: **else**
- 10: **break**;
- 11: **end if**
- 12: **end for**
- 13: **return** The reflection coefficients $\boldsymbol{\theta}^*$.

We will apply this algorithm in our experiments to obtain the near optimal reflection coefficients to configure the RIS.

V. EXPERIMENTAL RESULTS

A. Experimental Scenarios and Test Process

Our RIS-aided wireless communication system is composed of host Personal Computers (PCs), Universal Software Radio Peripherals (USRPs), RIS, and a control board. The whole system works at 5.8 GHz. The RIS board is composed of 512 elements, with 16 rows and 32 columns, each of which is quantized to 1-bit and designed the same as [10]. USRPs are used to process signal, and the control board is carefully designed to adjust the biased voltage of every individual

element of RIS. The detailed parameters of hardware are summarized in Table I.

TABLE I
DETAILED INFORMATION ON HARDWARE MODULES

Hardware configuration		Value
RIS element	Polarization	Unipolar
	Frequency	5.8 GHz
	Quantization	$\tau = 1$
	Spacing	$d_y = 14.3$ mm $d_z = 10.27$ mm
RIS board	Number of elements	16×32
	Control signal	Individual
Horn antenna	Gain	17.1 dBi @ 5.8 GHz
	Aperture	169 mm \times 119 mm
	Beamwidth	30°

Our experiments are made in indoor environment shown in Fig. 2. The RIS board is positioned against the wall, and the antennas of the base station and users are placed on one side of RIS and on the same horizontal plane. The transmitting horn antenna of the base station is perpendicular to the RIS, i.e., the angle of incidence is zeros. The distance between the antennas of the base station and the RIS, the k -th user and the RIS are denoted by d_b and d_k respectively. The antennas of users receive electromagnetic signals obliquely emitted by the RIS. Denote the angle between the receiving antenna of the k -th user and the center of the RIS by θ_k (let clockwise rotation be positive, and counterclockwise negative). The wave-absorbing material is placed at the left rear mainly to prevent the reflection from the iron gate.

According to the algorithm flow summarized in Section III and Section IV, our testing process will be divided into the following steps:

- (1) Initialization: Randomly generate reflection coefficients matrix following Rademacher distribution.
- (2) Setting: Transmit known pilots to all users.
- (3) Direct link estimation: Traditional LS channel estimation of direct link after turning off the RIS.
- (4) RIS-aided link estimation and reflection coefficients calculation: Turn on the RIS and switch the reflection coefficients of the RIS depending on the pre-generated Rademacher matrix, and at the same time the users sample received signal and reconstruct the cascaded channel vector based on the samples. With the objective of maximizing the spectral efficiency of the whole system, utilize the QTLM algorithm and calculate the reflection coefficients.
- (5) Beamforming: Apply the computed reflection coefficients to the RIS.

It is worth noting that, the estimation of the direct link can be solved by conventional LS method once we assume that the RIS absorbs the incident electromagnetic wave. In our experiments, in order to simply reach the state of absorption, we cover the RIS with wave-absorbing materials. However,

another approach to reach the same effect is illustrated in [32]. The work points out that, by tuning the resistance and reactance of the element, the input impedance of RIS can be changed, which will result in perfect absorption of the incident electromagnetic wave when it is matched with free-space impedance.

B. Channel Estimation Algorithm Experiments

For a single user RIS-aided communication system, the optimization problem is reduced from (P1) to

$$\begin{aligned} \max_{\boldsymbol{\theta}} \quad & \gamma = \frac{|h_d + \boldsymbol{\theta}^T \mathbf{h}_r|^2}{\sigma^2} \\ \text{s.t.} \quad & \theta_n \in \mathcal{F} \quad \forall n = 1, \dots, N. \end{aligned} \quad (40)$$

Once we obtain the channel state information of RIS-aided link, i.e., \mathbf{h}_r , the optimal reflection coefficients of RIS is approximately expressed as [17]

$$\boldsymbol{\theta}^{\text{SU}} = \frac{h_d}{|h_d|} \cdot \frac{\mathbf{h}_r^*}{\|\mathbf{h}_r\|}, \quad (41)$$

which straightforwardly concludes from the combination of Maximum Ratio Transmission (MRT) and phase alignment. If a quantized phase shifting scheme is taken into account, $\boldsymbol{\theta}$ is projected into the closest point from $\boldsymbol{\theta}^{\text{SU}}$ following the guidelines in (32). Therefore, the performance of the single-user system can reflect the accuracy of channel estimation algorithm, which can be observed by comparing the received power before and after the beamforming of RIS. The performance of the algorithm is reflected by a parameter G (dB) defined as

$$G \text{ (dB)} = 10 \log_{10} \left(\frac{P_r^{\text{B}}}{P_r^{\text{O}}} \right), \quad (42)$$

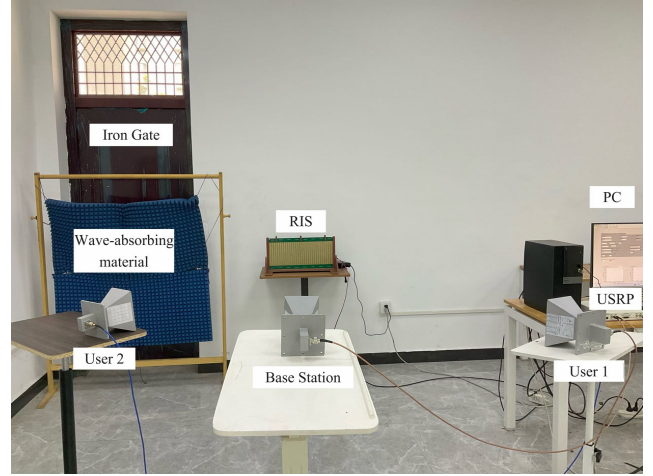
where P_r^{B} is the received power after configuring the beamforming of RIS and P_r^{O} is the received power when the RIS is powered off, which are both calculated from LabVIEW and follow

$$P_r \text{ (W)} = \frac{1}{N} \sum_{i=1}^N |x_i|^2, \quad (43)$$

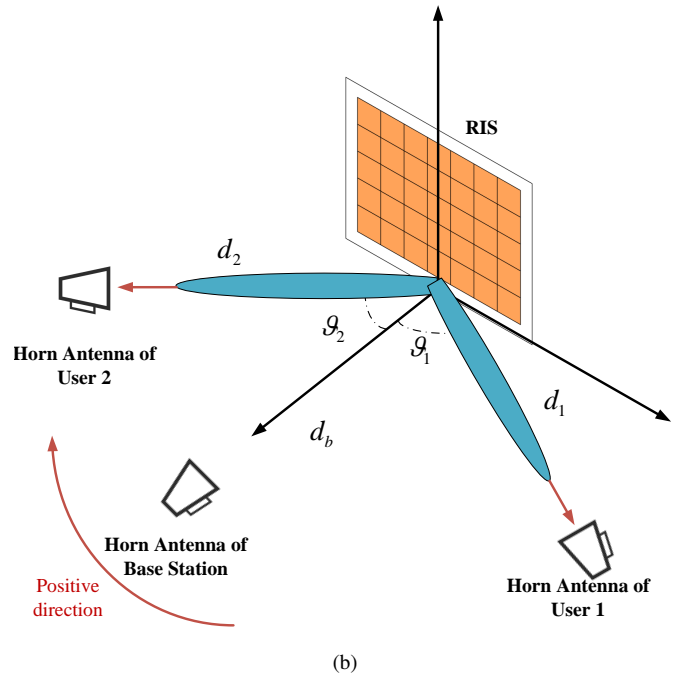
where x_i is the sample in the received frames, and N is the number of samples in a frame. Besides, when the relative locations of the user, the base station, and the RIS are fixed, the performance of the CS reconstructing algorithm suffers from influences of number of samples and signal power. Thus, we conduct two relevant types of experiments to verify the effectiveness of the proposed channel estimation algorithm.

The boundary of the near field and far field in our RIS model is around $B \simeq 2.9$ m according to (6). However, since the sparsity of angular channel model is not satisfied in the near field, the received power gain is lower compared with the far field scenarios. This effect is illustrated in Fig. 3. The average peak received power gain of the algorithm is 13.5 dB when the distance is 1.8 m, while the average peak received power gain is 27.9 dB when the distance is 2.3 m.

By changing the dimension of the sensing matrix in (11) when randomly generated, the algorithm utilizes different samples to recover the channel vector. It is also observed



(a)



(b)

Fig. 2. Indoor test scenario. (a) Real-world environment, (b) Location schematic.

in Fig. 3 that, as the number of samples increases, the received power gain of the single user grows gradually and the peak received power gain compared with the “OFF” state of RIS is 28.2 dB in such a single-user scenario. The curve tends to converge between 200 and 250 samples. Therefore, augmenting the number of samples beyond this range does not bring a performance enhancement for the channel estimation algorithm.

In order to observe the effect of signal power on algorithm performance, we conducted experiments in two strategies for the number of samples, i.e., $P = 100$ and $P = 300$, which corresponds to two curves in Fig. 4. To ensure the accuracy of the experiment, the measurement matrix is identical when the number of sampling points is the same. The increase of the signal power generally results in a performance gain, which

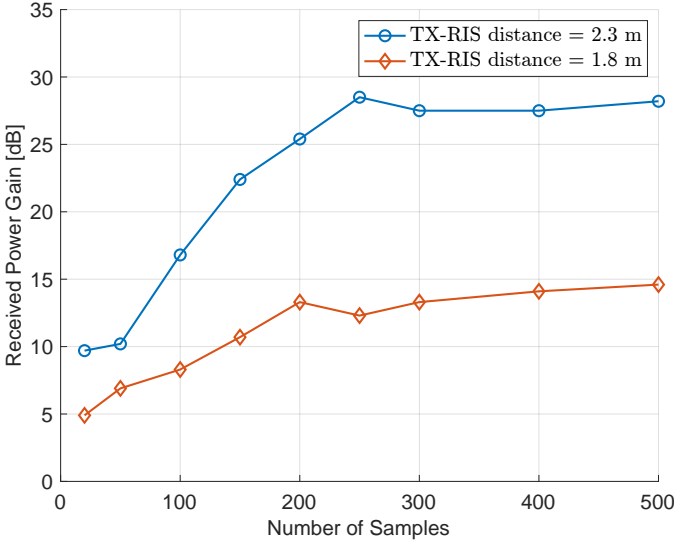


Fig. 3. Received power gain vs. number of samples in the single-user scenario, experiments settings are $d_1 = 2.50$ m, $\vartheta_1 = 25^\circ$.

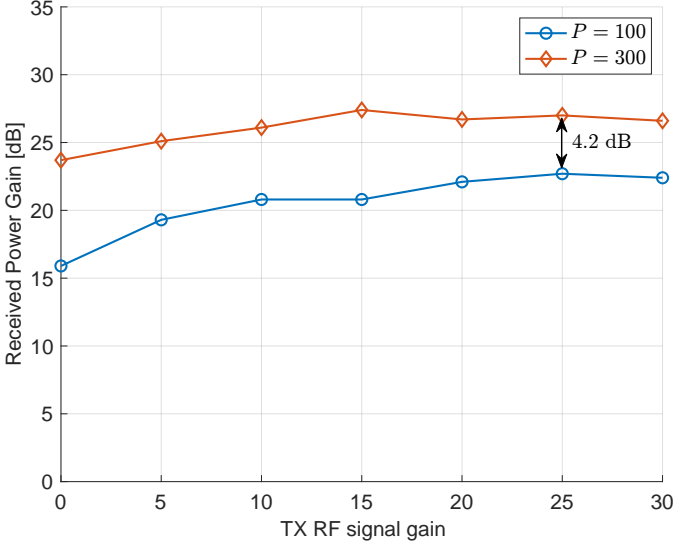


Fig. 4. Received power gain vs. TX RF signal gain in the single-user scenario, experiments settings are TX-RIS distance = 2.30 m, $d_1 = 2.60$ m, $\vartheta_1 = 22^\circ$.

is in line with the intuition of the EM-GAMP algorithm. In contrast, increasing the signal power when the number of samples is small is of greater importance. As can be seen from the two curves in the figure, in both cases, a 30 dB increase in transmitting signal power brings a 2.9 dB and 6.5 dB gain for the performance of the algorithm, respectively. There are also differences in the upper limits of the estimated performance of the measurement matrix for different dimensions, which is reflected by the received power gain gap of approximately 4.2 dB in Fig. 4.

C. Multi-user Passive Beamforming Experiments

1) *Correction on noise power:* In our passive beamforming algorithm, the noise power is needed at each iteration, i.e., the updating value of α in (20). Its accuracy will directly affect

the algorithm performance. We find that the noise floor in RF devices is insufficient for a complete measure of noise power, making the algorithm fail to compute the proper reflection coefficients results. Therefore, we take the defects in the RF chains into account, which is a different form of noise from Gaussian white noise and includes the influences of phase noise, noise figure, I/Q phase imbalance, and power supply noise. All these effects in the receiver can be reflected in the parameter of Receive Modulation Error Ratio (RxMER). One can calculate the average distance between the reference signal vector and measured signal vector in the constellation as RxMER in the following equation

$$\text{RxMER} = \frac{\sum_{i=1}^N |R_i|^2}{\sum_{i=1}^N |S_i - R_i|^2}, \quad (44)$$

where N is the number of samples in frames, S_i is the measured signal sample, and R_i is the reference signal sample. In this background, RxMER is a key indicator to quantify the transmitting performance of a wireless communication system, which measures Gaussian noise and other uncorrectable impairments of the received constellation [33].

Note that RxMER and SNR are equivalent when only Gaussian noise is present in the system. In other words, RxMER is a special manifestation of SNR. In the experiments, we can compute the RxMER value to substitute the noise floor part, which is equivalent to a correction for noise power. The correction value of noise power is

$$\bar{\sigma}^2 (W) = \frac{P_{r,k}}{\text{RxMER}}, \quad (45)$$

where $P_{r,k}$ is the average received power of the k -th user calculated in LabVIEW. In the later process of experiments, the noise correction value in (45) will be used instead of the noise floor for the calculation, making it as close to the true value as possible.

2) *Spectral efficiency of two users:* To illustrate the performance of the multi-user passive beamforming algorithm, we set up two users to conduct experiments. The relative location of all the transceivers is $(d_b, d_1, d_2, \theta_1, \theta_2) = (2.34$ m, 2.26 m, 2.00 m, $-28^\circ, 21^\circ)$. Since our objective is to maximize the spectral efficiency of the whole communication system for a multi-user situation, the effectiveness of the algorithm is reflected by the spectral efficiency defined as

$$S \text{ (bps/Hz)} = \sum_{k=1}^K \log_2 \left(1 + \frac{P_{r,k}}{\sigma^2} \right), \quad (46)$$

where $P_{r,k}$ is the average received power of the k -th user after beamforming of the RIS.

Similarly, we change experimental conditions, and a figure of the variation of the spectral efficiency with the number of samples and the TX RF signal gain was obtained (the points in the figure with the number of samples of 0 indicate the spectral efficiencies when the RIS is powered off). Fig. 5 shows that, as the number of samples grows, the spectral efficiency of the whole communication system increases. The saturation point of the system capacity is between 250 and 300, and then increasing the number of samples does not deliver a noticeable

performance boost. Increasing the number of samples from 20 to 500 gives the system an average spectral efficiency increase of 6.15 bps/Hz. If compared with the situation when the RIS is powered off, the average spectral efficiency gain grows to 13.48 bps/Hz.

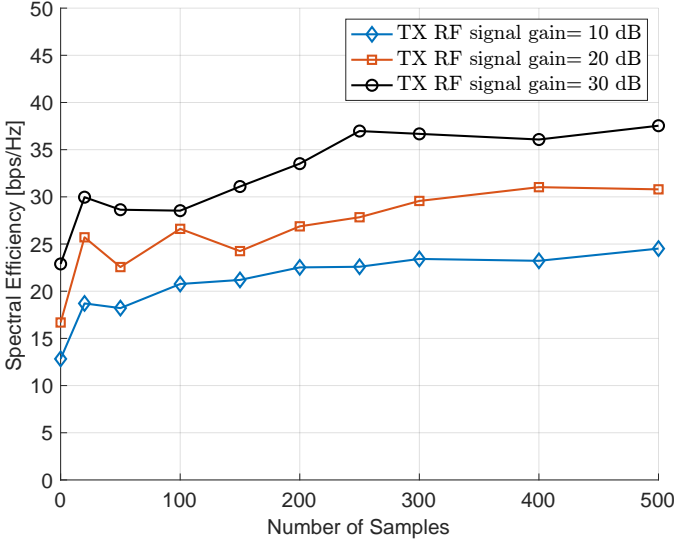


Fig. 5. The spectral efficiency after configuring reflection coefficients of RIS under the different numbers of samples and TX RF signal gains, the points with the number of samples of 0 indicate the spectral efficiencies when the RIS is powered off.

The received power gains of each user in different experimental configurations are also recorded in Table II. Fig. 6 shows the spectrum and average received power of two users before and after beamforming of the RIS, when the number of samples is 500 and the TX RF signal gain is 30 dB. The received powers of two users when the RIS is powered off are -51.5 dBW and -43.6 dBW respectively. After configuring the reflection coefficients of the RIS, the received power grows to -24.9 dBW and -26.1 dBW. The two users obtain the gains of 26.6 dB and 17.5 dB comparing with the powered-off case. The results reveals that the QTLM algorithm makes a decent balance between two users when their respective channel quality is similar, resulting in received power gains of around the same magnitude. However, we also observed that when one of users is in a low-quality environment, the inaccurate channel will interfere with another user in the process of the beamforming algorithm, causing the final throughput rate to not increase as much as expected.

3) *Radiation Pattern*: For an RIS-aided multi-user communication system, the improvement of spectral efficiency also indicates the multi-beam performance of RIS. Therefore, we conduct radiation pattern experiments in a microwave anechoic chamber as shown in Fig. 7. The transmitting antenna and the RIS are fixed on a rotating platform, while the received antenna is fixed on a table and face the RIS.

We used the results obtained from the multi-user experiments conducted above, i.e., the location information is $(d_b, d_1, d_2, \theta_1, \theta_2) = (2.34 \text{ m}, 2.26 \text{ m}, 2.00 \text{ m}, -28^\circ, 21^\circ)$, and measured the radiation pattern of the codeword. The platform rotated and the received powers was recorded in every

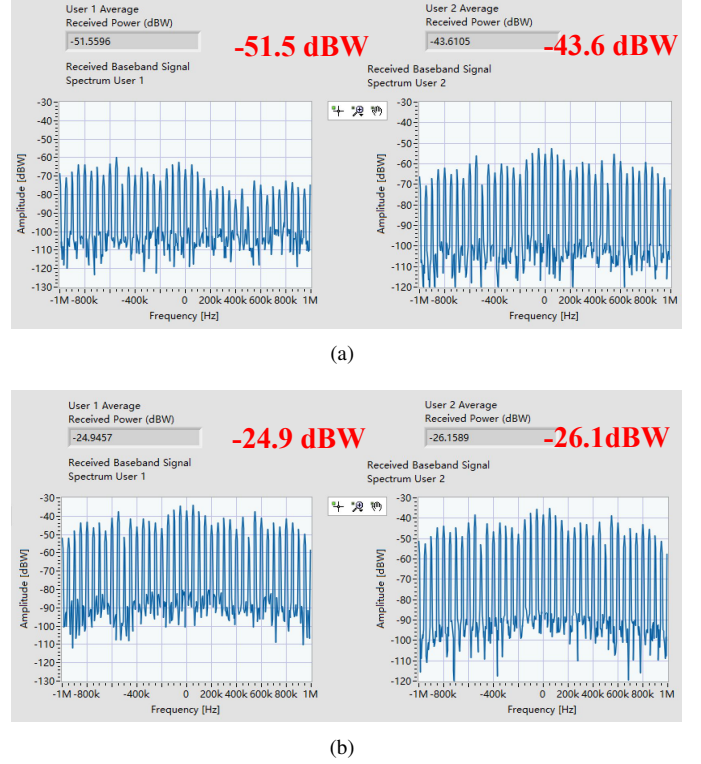


Fig. 6. Average received power and spectrum of RX baseband signal for two users obtained from LabVIEW. The experimental results are obtained when $P = 500$, TX RF signal gain = 30 dB. (a) All the RIS elements are powered off. (b) After configuring reflection coefficients of the RIS.

TABLE II
RECEIVED POWER GAIN OF EACH USER
COMPARED WITH RIS POWERED OFF

TX Gain	10 dB		20 dB		30 dB	
	user1	user2	user1	user2	user1	user2
20	5.4	12.4	13.3	13.9	13.0	8.3
50	6.5	9.8	2.7	15.0	5.2	12.1
100	7.7	16.3	11.3	18.6	10.5	6.5
150	11.5	13.8	8.1	14.7	11.6	13.1
200	12.1	17.2	16.2	14.5	19.8	12.2
250	9.1	20.4	23.0	10.6	27.0	15.4
300	6.5	17.8	21.9	16.9	27.3	14.2
400	13.7	17.7	23.4	19.8	25.7	14.0
500	16.7	18.6	22.8	19.7	26.6	17.5

azimuth direction. The TX-RIS distance is 0.4 m, and the RIS-RX distance is 2.2 m. The reason that TX-RIS distance does not keep the same as experimental scenario is the length extension limitation of the rotation platform. The radiation pattern of the corresponding codeword is shown in Fig. 8, where the maximum gain is normalized to 0 dB. The half-power beamwidth is 9.22° . It can be observed that there are two wave peaks in radiation pattern, the angle of which are approximately located at -28° and 21° , which corresponds exactly to our experimental scenario. This pattern implies the

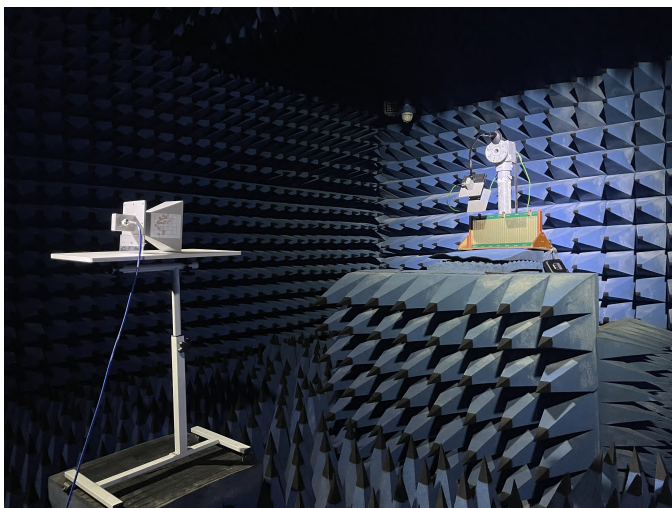


Fig. 7. The microwave anechoic chamber of size 4 m \times 6 m \times 4 m, the TX-RIS distance is 0.4 m, the RIS-RX distance is 2.2 m.

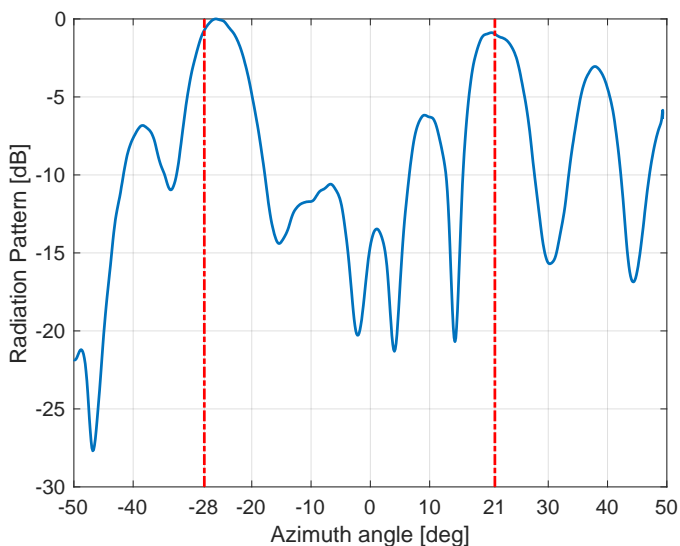


Fig. 8. Measured normalized radiation pattern of RIS with reflection coefficients obtained from the last section.

multi-beam capability of the RIS board and the multi-user effectiveness of the algorithms.

VI. CONCLUSION

In this paper, we proposed a multi-user beamforming scheme for an RIS-aided wireless communication system and implemented all the algorithms in our prototype for the experimental validations. By introducing the angular domain channel model, we solved the channel estimation problem with compressed sensing, and proposed to generate the measurement matrix with Rademacher distribution to match the 1-bit RIS prototype and utilized the EM-GAMP algorithm to reconstruct the sparse signal. To generate the reflection coefficients of RIS in multi-user scenarios, we proposed a QTLM algorithm, which exploits the structural properties of the channel to enhance convergence speed and reduce complexity. To address RF device imperfections, we put forth a novel method for

correcting noise power values, ensuring the efficacy of our algorithms within the RIS prototype. By conducting the experiments with the fabricated RIS prototype system, we verified the effectiveness of all proposed algorithms. The results reveal that the RIS can bring a noticeable increase on the spectral efficiency of the whole multi-user system with our proposed algorithms.

REFERENCES

- [1] Q. Wu and R. Zhang, "Towards smart and reconfigurable environment: Intelligent reflecting surface aided wireless network," *IEEE Commun. Mag.*, vol. 58, no. 1, pp. 106–112, 2019.
- [2] M. Di Renzo, A. Zappone, M. Debbah, M.-S. Alouini, C. Yuen, J. De Rosny, and S. Tretyakov, "Smart radio environments empowered by reconfigurable intelligent surfaces: How it works, state of research, and the road ahead," *IEEE J. Sel. Areas Commun.*, vol. 38, no. 11, pp. 2450–2525, 2020.
- [3] C. Pan, H. Ren, K. Wang, J. F. Kolb, M. Elkashlan, M. Chen, M. Di Renzo, Y. Hao, J. Wang, A. L. Swindlehurst *et al.*, "Reconfigurable intelligent surfaces for 6G systems: Principles, applications, and research directions," *IEEE Commun. Mag.*, vol. 59, no. 6, pp. 14–20, 2021.
- [4] N. Rajatheva, I. Atzeni, E. Bjornson, A. Bourdoux, S. Buzzi, J.-B. Dore, S. Erkucuk, M. Fuentes, K. Guan, Y. Hu *et al.*, "White paper on broadband connectivity in 6g," *arXiv preprint arXiv:2004.14247*, 2020.
- [5] C. Liaskos, S. Nie, A. Tsioliaridou, A. Pitsillides, S. Ioannidis, and I. Akyildiz, "A new wireless communication paradigm through software-controlled metasurfaces," *IEEE Commun. Mag.*, vol. 56, no. 9, pp. 162–169, 2018.
- [6] T. Cui, M. Qi, X. Wan, J. Zhao, and Q. Cheng, "Coding metamaterials, digital metamaterials and programmable metamaterials," *Light-Sci. Appl.*, vol. 3, no. 10, pp. e218–e218, 2014.
- [7] L. Zhang, X. Chen, S. Liu, Q. Zhang, J. Zhao, J. Dai, G. Bai, X. Wan, Q. Cheng, G. Castaldi *et al.*, "Space-time-coding digital metasurfaces," *Nat. Commun.*, vol. 9, no. 1, p. 4334, 2018.
- [8] L. Zhang, X. Chen, R. Shao, J. Dai, Q. Cheng, G. Castaldi, V. Galdi, and T. Cui, "Breaking reciprocity with space-time-coding digital metasurfaces," *Adv. Mater.*, vol. 31, no. 41, p. 1904069, 2019.
- [9] L. Dai, B. Wang, M. Wang, X. Yang, J. Tan, S. Bi, S. Xu, F. Yang, Z. Chen, M. Di Renzo *et al.*, "Reconfigurable intelligent surface-based wireless communications: Antenna design, prototyping, and experimental results," *IEEE Access*, vol. 8, pp. 45 913–45 923, 2020.
- [10] X. Pei, H. Yin, L. Tan, L. Cao, Z. Li, K. Wang, K. Zhang, and E. Björnson, "RIS-aided wireless communications: Prototyping, adaptive beamforming, and indoor/outdoor field trials," *IEEE Trans. Commun.*, vol. 69, no. 12, pp. 8627–8640, 2021.
- [11] W. Tang, M. Chen, X. Chen, J. Dai, Y. Han, M. Di Renzo, Y. Zeng, S. Jin, Q. Cheng, and T. Cui, "Wireless communications with reconfigurable intelligent surface: Path loss modeling and experimental measurement," *IEEE Trans. Wireless Commun.*, vol. 20, no. 1, pp. 421–439, 2020.
- [12] Z. Wang, L. Tan, H. Yin, K. Wang, X. Pei, and D. Gesbert, "A received power model for reconfigurable intelligent surface and measurement-based validations," in *2021 IEEE 22nd International Workshop on Signal Processing Advances in Wireless Communications (SPAWC)*, 2021, pp. 561–565.
- [13] F. H. Danufane, M. Di Renzo, J. De Rosny, and S. Tretyakov, "On the path-loss of reconfigurable intelligent surfaces: An approach based on green's theorem applied to vector fields," *IEEE Trans. Commun.*, vol. 69, no. 8, pp. 5573–5592, 2021.
- [14] S. Lin, B. Zheng, G. C. Alexandropoulos, M. Wen, F. Chen *et al.*, "Adaptive transmission for reconfigurable intelligent surface-assisted OFDM wireless communications," *IEEE J. Sel. Areas Commun.*, vol. 38, no. 11, pp. 2653–2665, 2020.
- [15] B. Zheng and R. Zhang, "Intelligent reflecting surface-enhanced OFDM: Channel estimation and reflection optimization," *IEEE Wireless Commun. Lett.*, vol. 9, no. 4, pp. 518–522, 2019.
- [16] Y. Yang, B. Zheng, S. Zhang, and R. Zhang, "Intelligent reflecting surface meets OFDM: Protocol design and rate maximization," *IEEE Trans. Commun.*, vol. 68, no. 7, pp. 4522–4535, 2020.
- [17] Q. Wu and R. Zhang, "Intelligent reflecting surface enhanced wireless network via joint active and passive beamforming," *IEEE Trans. Wireless Commun.*, vol. 18, no. 11, pp. 5394–5409, 2019.

- [18] H. Guo, Y.-C. Liang, J. Chen, and E. G. Larsson, "Weighted sum-rate optimization for intelligent reflecting surface enhanced wireless networks," *arXiv preprint arXiv:1905.07920*, 2019.
- [19] X. Ma, S. Guo, H. Zhang, Y. Fang, and D. Yuan, "Joint beamforming and reflecting design in reconfigurable intelligent surface-aided multi-user communication systems," *IEEE Trans. Wireless Commun.*, vol. 20, no. 5, pp. 3269–3283, 2021.
- [20] S. Ren, K. Shen, Y. Zhang, X. Li, X. Chen, and Z.-Q. Luo, "Configuring intelligent reflecting surface with performance guarantees: Blind beamforming," *IEEE Trans. Wireless Commun.*, vol. 22, no. 5, pp. 3355 – 3370, 2022.
- [21] M. Ouyang, F. Gao, Y. Wang, S. Zhang, P. Li, and J. Ren, "Computer vision-aided reconfigurable intelligent surface-based beam tracking: prototyping and experimental results," *IEEE Trans. Wireless Commun.*, 2023.
- [22] R. Xiong, J. Zhang, X. Dong, Z. Wang, J. Liu, T. Mi, and R. C. Qiu, "RIS-aided wireless communication in real-world: Antennas design, prototyping, beam reshape and field trials," *arXiv preprint arXiv:2303.03287*, 2023.
- [23] M. M. Amri, N. M. Tran, and K. W. Choi, "Reconfigurable intelligent surface-aided wireless communications: Adaptive beamforming and experimental validations," *IEEE Access*, vol. 9, pp. 147 442–147 457, 2021.
- [24] X. Wei, D. Shen, and L. Dai, "Channel estimation for RIS assisted wireless communications—part II: An improved solution based on double-structured sparsity," *IEEE Commun. Lett.*, vol. 25, no. 5, pp. 1403–1407, 2021.
- [25] H. Yin, D. Gesbert, M. Filippou, and Y. Liu, "A coordinated approach to channel estimation in large-scale multiple-antenna systems," *IEEE J. Sel. Areas Commun.*, vol. 31, no. 2, pp. 264–273, 2013.
- [26] A. A. Saleh and R. Valenzuela, "A statistical model for indoor multipath propagation," *IEEE J. Sel. Areas Commun.*, vol. 5, no. 2, pp. 128–137, 1987.
- [27] A. Meijerink and A. F. Molisch, "On the physical interpretation of the saleh–valenzuela model and the definition of its power delay profiles," *IEEE Trans. Antennas Propag.*, vol. 62, no. 9, pp. 4780–4793, 2014.
- [28] H. Yin, H. Wang, Y. Liu, and D. Gesbert, "Addressing the curse of mobility in massive MIMO with prony-based angular-delay domain channel predictions," *IEEE J. Sel. Areas Commun.*, vol. 38, no. 12, pp. 2903–2917, 2020.
- [29] E. J. Candès, J. Romberg, and T. Tao, "Robust uncertainty principles: Exact signal reconstruction from highly incomplete frequency information," *IEEE Trans. Inf. Theory*, vol. 52, no. 2, pp. 489–509, 2006.
- [30] J. A. Tropp and A. C. Gilbert, "Signal recovery from random measurements via orthogonal matching pursuit," *IEEE Trans. Inf. Theory*, vol. 53, no. 12, pp. 4655–4666, 2007.
- [31] K. Shen and W. Yu, "Fractional programming for communication systems—part I: Power control and beamforming," *IEEE Trans. Signal Process.*, vol. 66, no. 10, pp. 2616–2630, 2018.
- [32] M. F. Imani, D. R. Smith, and P. del Hougne, "Perfect absorption in a metasurface-programmable complex scattering enclosure," *arXiv preprint arXiv:2003.01766*, 2020.
- [33] R. Hranac, "Digital transmission: Carrier-to-noise ratio, signal-to-noise ratio, and modulation error ratio," *Broadcom Corporation and Cisco Systems, white paper*, 2006.